Journal of Materials Science: Materials in Electronics (2018) 29:19123–19129
https://doi.org/10.1007/s10854-018-0038-5

Excellent optical, dielectric, and ferroelectric properties of $Sr(In_{0.5}Nb_{0.5})O_3$ modified $K_{0.5}Na_{0.5}NbO_3$ lead-free transparent ceramics

Hang Xie[1] · Guobao Liu[1] · Ling Yang[1] · Sijian Pang[1] · Changlai Yuan[1,2] · Xiaowen Zhang[1,2] · Hua Wang[1,2] · Changrong Zhou[1,2] · Jiwen Xu[1,2]

Received: 6 August 2018 / Accepted: 8 September 2018 / Published online: 22 September 2018

Abstract
High visible light transmittance $(1-x)(K_{0.5}Na_{0.5})NbO_3-xSr(In_{0.5}Nb_{0.5})O_3$ (KNN−*x*SIN, $x=0.05, 0.10, 0.15, 0.20, 0.25$) lead-free ceramics with excellent electrical properties were synthesized by traditional solid-state method. The effects of $Sr(In_{0.5}Nb_{0.5})O_3$ doping on the optical properties, microstructure, and electrical performance were analyzed. The results showed that light transmission in KNN−*x*SIN ceramics was induced by the dense and fine-grain microstructure, the high symmetry of the pseudo-cubic structure as well as typical relaxor behavior of KNN−0.25SIN ceramic. Moreover, KNN−*x*SIN transparent ceramics with relaxor characteristics possessed permittivity stability over a wide temperature range. Ferroelectric properties were deteriorated gradually with increasing SIN content in virtue of the strengthened relaxor behavior. Its energy storage property was also tailored by the increasing relaxor characteristic. The appearance of a non-Debye type of relaxation was detected through an impedance Cole–Cole plots.

1 Introduction

Transparent electronic ceramic is a new type of materials with excellent optical and electrical performance, which is extensively applied in modern information technology, future optical computer technology, and advanced control technology [1–3]. Among them, the most representative one is (Pb, La)(Zr, Ti)O_3 (PLZT) transparent ferroelectric ceramics fabricated by a hot-pressing process in 1972 [4], which not only has high transmittance, but also possesses piezoelectric and ferroelectric characteristics after being poled, and has many electrical and optical applications, such as light modulator and multifunction compact devices [5, 6]. However, PLZT ceramics containing high content of hazardous substances have been prohibited due to the increasing healthy and environmental concerns. So it is of great importance to develop new lead-free transparent electronic ceramics.

Since the discussion of optical characteristics in $0.8(K_{0.5}Na_{0.5})NbO_3-0.2SrTiO_3$ ceramics emerged in 2004 [7], a large and growing body of literatures have focused on the KNN-based transparent ceramics. Li et al. employed a hot-pressing method to fabricate $K_{0.48}Na_{0.52}Nb_{1-x}Bi_xO_3$ ceramics with 80% transmittance at 4000 nm [8]. The $(K_{0.5}Na_{0.5})_{0.95}Li_{0.05}Nb_{0.95}Bi_{0.05}O_3$ transparent ceramics fabricated by hot-pressing sintering had 60% transmittance in the near-IR region [9]. However, the high cost of hot-pressing sintering method is not suitable for industrial applications. The crystal symmetry is a crucial issue that has a vital influence on the optical properties of ceramics. It is discovered that a quantity of transparent ceramics with excellent transmittance possess high symmetry cubic phase as a result of the weakness of light scattering. Nevertheless, the ferroelectric properties of ferroelectric ceramics mainly stem from the lower symmetry of the crystal structure, which means that it is arduous to acquire the ferroelectric ceramics with optimal transmittance simultaneously. So study on the excellent electrical properties of ferroelectric ceramics with high transmittance becomes necessary. For the investigation of

✉ Hua Wang
wh65@guet.edu.cn

✉ Jiwen Xu
csuxjw@126.com

[1] School of Materials Science and Engineering, Guilin University of Electronic Technology, Guilin 541004, People's Republic of China

[2] Guangxi Key Laboratory of Information Materials, Guilin University of Electronic Technology, Guilin 541004, People's Republic of China

KNN-based ceramics, ion substitution method is used to solve the above contradiction. The replacement of aliovalent ions at A-site could enhance the electrical properties of KNN-based ceramics due to the diverse defect structure [10–12]. Besides, aliovalent ions also can be adopted to regulate its electrical properties by shaping point defects at B-site [13–15]. According to the above analysis, here, we investigate a new $(1-x)(K_{0.5}Na_{0.5})NbO_3-xSr(In_{0.5}Nb_{0.5})O_3$ lead-free transparent ceramic by traditional solid-phase sintering route, which possesses both high transmittance and excellent electrical properties simultaneously.

Introducing other solid solution into KNN-based lead-free ceramics can contribute to relaxor behavior and thus become a crucial issue to achieve excellent optical performance [9, 16, 17]. Analogous to the $Pb(In_{0.5}Nb_{0.5})O_3$-based perovskite type ferroelectric ceramics with relaxor behavior, here, $Sr(In_{0.5}Nb_{0.5})O_3$ was selected and added into KNN ceramics to form the relaxor behavior [18, 19]. Besides, the valence and ionic radius of Sr^{2+} (1.18 Å) are different from those of $(K_{0.5}Na_{0.5})^+$ (1.2 Å) in A-site cations. A similar case also exists in B-site cations, where In^{3+} (0.8 Å) and Nb^{5+} (0.64 Å) also possess distinct valence and radii. The imbalanced valence and different radii in A/B-sites cations can form the locally distorted crystal lattice, which contributes to the polar nanoregions (PNRs) related to the relaxation behavior of ferroelectrics [1]. The objective of this work, therefore, is to explore the effect of SIN level on the microstructure, optical, and electrical behaviors of KNN–*x*SIN ceramics, which is beneficial to constructing the desirable electrical properties with a high visible light transmittance in KNN-based lead-free ceramics.

2 Experimental

Na_2CO_3 (99.80%), K_2CO_3 (99.00%), Nb_2O_5 (99.95%), $SrCO_3$ (99.99%), and In_2O_3 (99.99%) were used to fabricate KNN–*x*SIN transparent ceramics by conventional solid phase approach. The powders, mixed with ethanol as media, were ball-milled drastically for 24 h. The dried powders were calcined at 950 °C for 5 h and then calcined at the same condition again after being ground evenly. The calcined powders were pressed into disks with a diameter of 13 mm under 10 MPa. The green bodies, surrounded by some calcined powders as sintering atmosphere, were sintered at 1200–1270 °C for 5 h in double sealed alumina crucibles. Finally, the obtained samples were polished to 0.5 mm thickness.

The crystalline structure was recorded by X-ray diffraction (XRD, Bruker, Germany). The microstructure was observed by field-emission scanning electron microscopy (FESEM, quanta 450 FEG, FEI). The transmittance was detected via UV–Vis spectrophotometer (UV-6100, Metash, China). An impedance analyzer (4294A, Agilent) was used to determinate the dielectric properties, and it was also used to measure the temperature dependent impedance spectrum from 40 Hz to 1 MHz. Dielectric-temperature spectra of high (25–450 °C) and low (− 75 to 200 °C) temperatures are tested separately because the equipment uses different test fixtures. Hysteresis loops (*P*–*E*) were tested by ferroelectric materials measurement system (P-PMF, Radiant).

3 Results and discussion

Figure 1a presents the optical transmittance (*T*) of KNN–*x*SIN ceramics, and the optimal photograph of KNN–0.25SIN ceramic is displayed in Fig. 1b. As shown in Fig. 1a, the SIN content makes a significant effect on the transmittance of KNN–*x*SIN ceramics, and its transmittance increases gradually when the SIN content rises from 0.05 to 0.25 in the measured wavelength region. It also can be seen from Fig. 1a that the KNN–0.25SIN composition illustrates higher transmittance. Its transmittance in the visible spectra exceeds 40%, and reaches 66% at 1100 nm. It was estimated that the optical transparency can be optimized by optical-grade polishing in the visible light range [9, 20]. If the reflection loss existing at the interface between air and ceramics can be weakened through the appropriate component, the optical transparency of the KNN–SIN

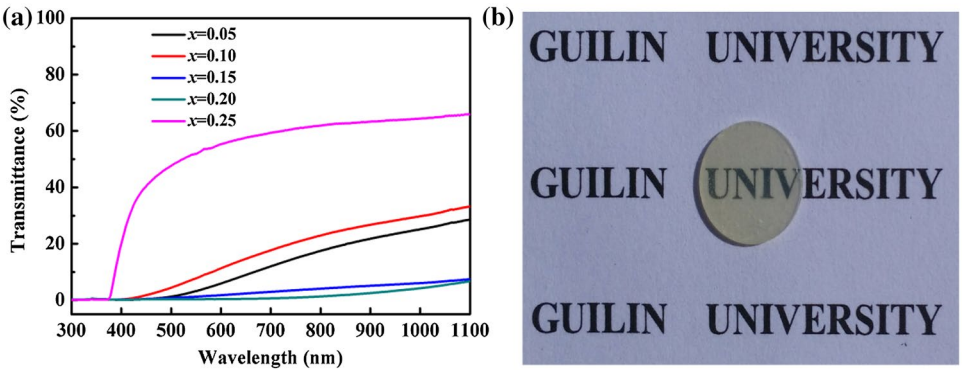

Fig. 1 **a** Optical transmission characteristics of the KNN–*x*SIN ceramics, **b** photograph of the KNN–0.25SIN ceramic

ceramics will be promoted even more [21]. As displayed in Fig. 1b, the tagged symbol under the optimal sample for KNN−0.25SIN ceramic can be viewed distinctly, suggesting that this optimal composition has the best transmittance within the measurement range.

Further analysis indicates that the transmittance is close to zero at 400 nm or below, implying that high absorption existed in the short wavelength range is related to the inter-band gap energy [22]. The calculated optical band gap energy (E_g) is based on the absorption spectra according to the Tauc equation [23]. The correlation between E_g and absorption coefficient α can be induced by the following Eq. (1):

$$(\alpha h\nu) = A\left(h\nu - E_g\right)^2 \tag{1}$$

where ν, h correspond to photon frequency and Planck's constant, respectively. A is a constant. In addition, α could be obtained according to the Eq. (2):

$$\alpha = \left(\frac{1}{t}\right)\ln\left(\frac{1}{T}\right) \tag{2}$$

where t and T are the thickness and transmittance of the tested samples, respectively. Figure 2 shows the plots of $(\alpha h\nu)^2$ versus $h\nu$, and the interception arising from the outstretched linear part of the curve to zero represents E_g, as described in reference [24]. It is apparent that E_g varies significantly from 2.33 to 3.22 eV, suggesting that SIN doping exerts a strong influence on the band gap energy of the KNN−xSIN ceramics. As shown in Fig. 2f, the E_g fluctuates around 2.5 eV with the increasing of SIN, and KNN−0.25SIN ceramic achieves the biggest value of 3.22 eV finally. Such result is far greater than that of other KNN-based transparent ceramics [25–28]. The band gap energy of KNN-based transparent ceramics is confirmed by the electron occupied state of NbO_6 octahedral, that is the transition from the O_{2p} electron at the top valence bands to the Nb_{4d} states occupied at the bottom of conduction bands [17, 29]. Moreover, according to these references [17, 30], the introducing of Sr^{2+} cations expands the band gap.

The optical transmittance can also be determined by crystal structure. Generally speaking, because of its single refractive index, the obtained ceramics with a cubic-like perovskite structure display better optical transmittance. Thus, when incident light passes through the grain boundaries of the crystal with an isotropic lattice structure, the scattering intensity of incident light would be attenuated [1]. Figure 3a shows the XRD diffraction patterns of KNN−xSIN ceramics. With the increase of SIN content, KNN−xSIN ceramics all show pure perovskite structure without any other miscellaneous peaks, meaning that SIN is thoroughly dissolved into the lattice of KNN matrix, and thus a new perovskite-type solid solution of KNN−xSIN ceramics is achieved. Furthermore, the phase structure characterizes the pseudo-cubic phase for KNN−xSIN ceramics without marked variation, which can be demonstrated by the no-split (200) peak from 44.5° to 46.5°, as exhibited in Fig. 3b [21]. The anisotropy of the samples with high symmetrical pseudo-cubic phase structure

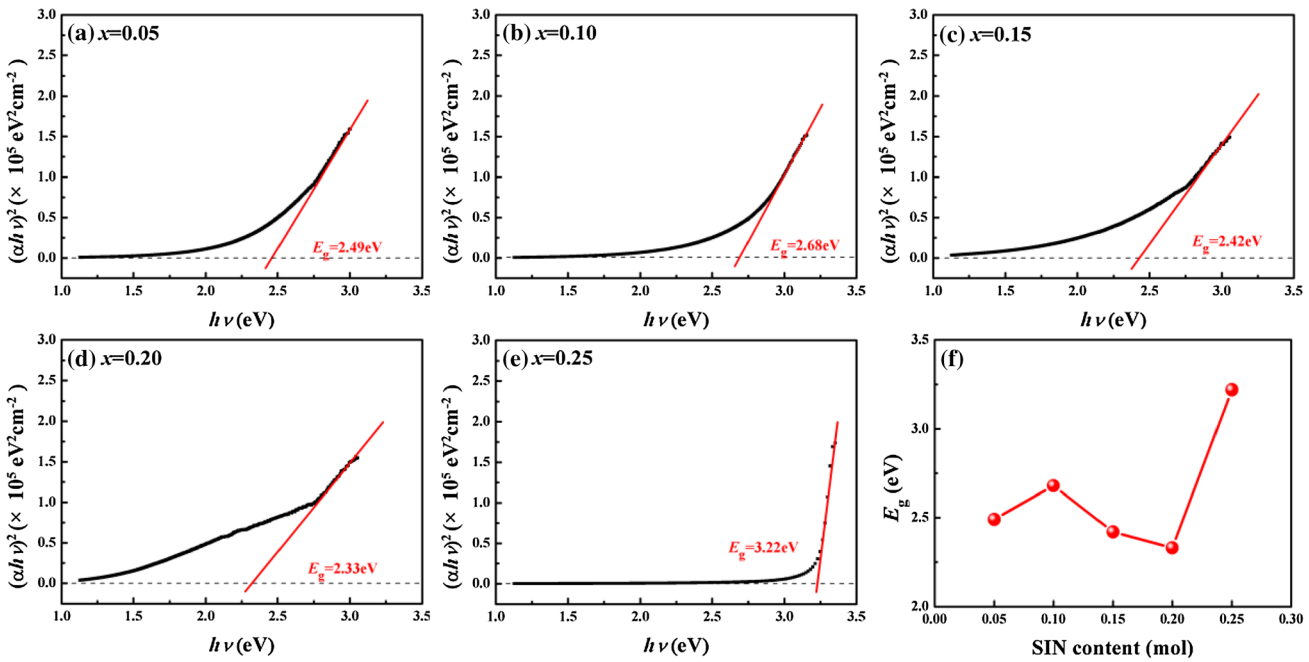

Fig. 2 **a**–**e** Plots of $(\alpha h\nu)^2$ versus $h\nu$, and **f** energy band gap E_g for the KNN−xSIN ceramics

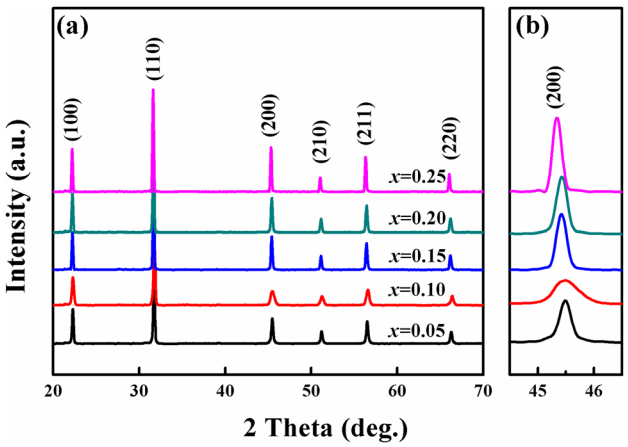

Fig. 3 XRD patterns of KNN−*x*SIN ceramics

was at the modest degree, resulting in smaller light scattering as well as the enhancement of the optical transmittance. Gradually, the (200) peak shifts toward the lower angle direction, which indicates an increasing lattice parameter. The difference of the cations radius between the bigger In^{3+} (0.8 Å) and smaller Nb^{5+} (0.64 Å) at B-site may be obligated to the cell lattice expansion.

Figure 4a, b show the SEM photographs of KNN−0.25SIN powder and ceramic samples, respectively. It can be seen from Fig. 4a that the powder has sub-micron size about 200 nm, high specific surface area and regular spherical soft agglomeration morphology, which indicates the good fluidity and high sintering activity of powder. The powder has no obvious reunion phenomenon, and good dispersion is propitious to the sintering of the green body and reducing the pores of the ceramics. Figure 4b shows the typical SEM micrograph of KNN−0.25SIN ceramic, which exhibits dense microstructures with ignorable pores, submicron fine grains, and cubic-like morphology grains. As we know, grain microstructure and porosity controlling the uniformity of microstructure, are commonly believed to be the vital factors affecting the transparency of ceramics [20]. In addition, the calculated average grain size is about 0.36 μm. As the Tyndall effect goes that much smaller grain size is hard to produce severe scattering and reflection phenomena [2].

Figure 5 demonstrates temperature dependence of dielectric properties for KNN−*x*SIN ceramics at 1 kHz, 10 kHz and 100 kHz. It can be seen that increasing SIN solid solution content can reduce dielectric constant. In the low-temperature region, the dielectric constant has a certain degree of dependence on the frequency, indicating that the KNN−*x*SIN ceramics have the characteristics of frequency dispersion. As the temperature rises, frequency dependence of dielectric constant becomes less obvious. The dielectric constant curves overlap finally with SIN content increasing, indicating that the dependence of KNN−*x*SIN ceramics on frequency is weakened. Dielectric loss exhibits opposite characteristics to frequency. Due to space charge polarization, dielectric loss increases sharply at higher temperatures, which can be illustrated by Shockley–Read mechanism [31–33]. Moreover, the existing of the diffuse phase transition feature can be determined by shifting of maximum permittivity temperature (T_m) towards low-temperature direction and broaden peaks with increasing SIN content. The relaxor characteristics of dielectric permittivity, which are consisted of the synchronous diffuse phase transition and frequency dispersion, illustrate that KNN−*x*SIN ceramics are of typical relaxor ferroelectrics materials. Qu et al. reported that the relaxor behavior is derived from local distortion of the lattice in relaxor ferroelectrics, accounting for the generation of polar nanoregions (PNRs) [1]. A surge of PNRs will lead to the formation of the pseudo-cubic structure and reduces the optical anisotropy of crystal, which can weaken the scattering of light when the light travels through the grain boundaries, and thus ferroelectric ceramics with relaxor behavior have optimal optical transparency. Specifically, dielectric properties of KNN−*x*SIN ceramics ($0.10 \le x \le 0.20$) exhibit temperature stability from − 50 to 200 °C. The temperature coefficient of permittivity ($TC\varepsilon$) can be calculated by the relative dielectric constant data of the corresponding composition at 1 kHz [34]. In order to obtain the best performance of the high-temperature capacitor, the ideal $TC\varepsilon$ is anticipated to be zero. Here, $TC\varepsilon$ for KNN−0.10SIN, KNN−0.15SIN and KNN−0.20SIN

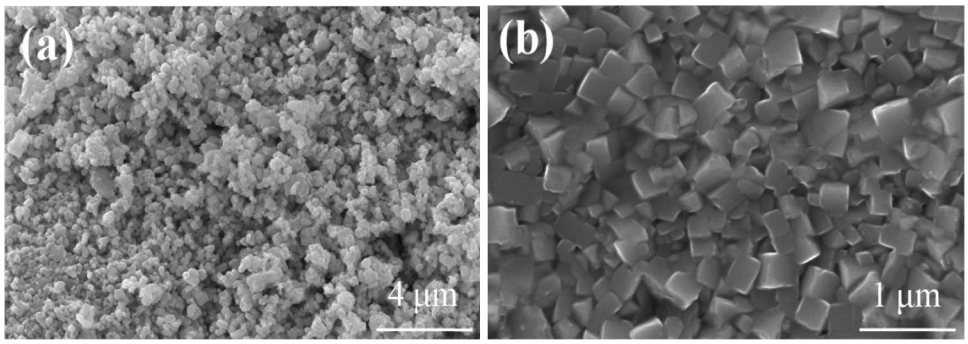

Fig. 4 The microscope photographs of **a** KNN−0.25SIN calcined powder and **b** KNN−0.25SIN ceramic

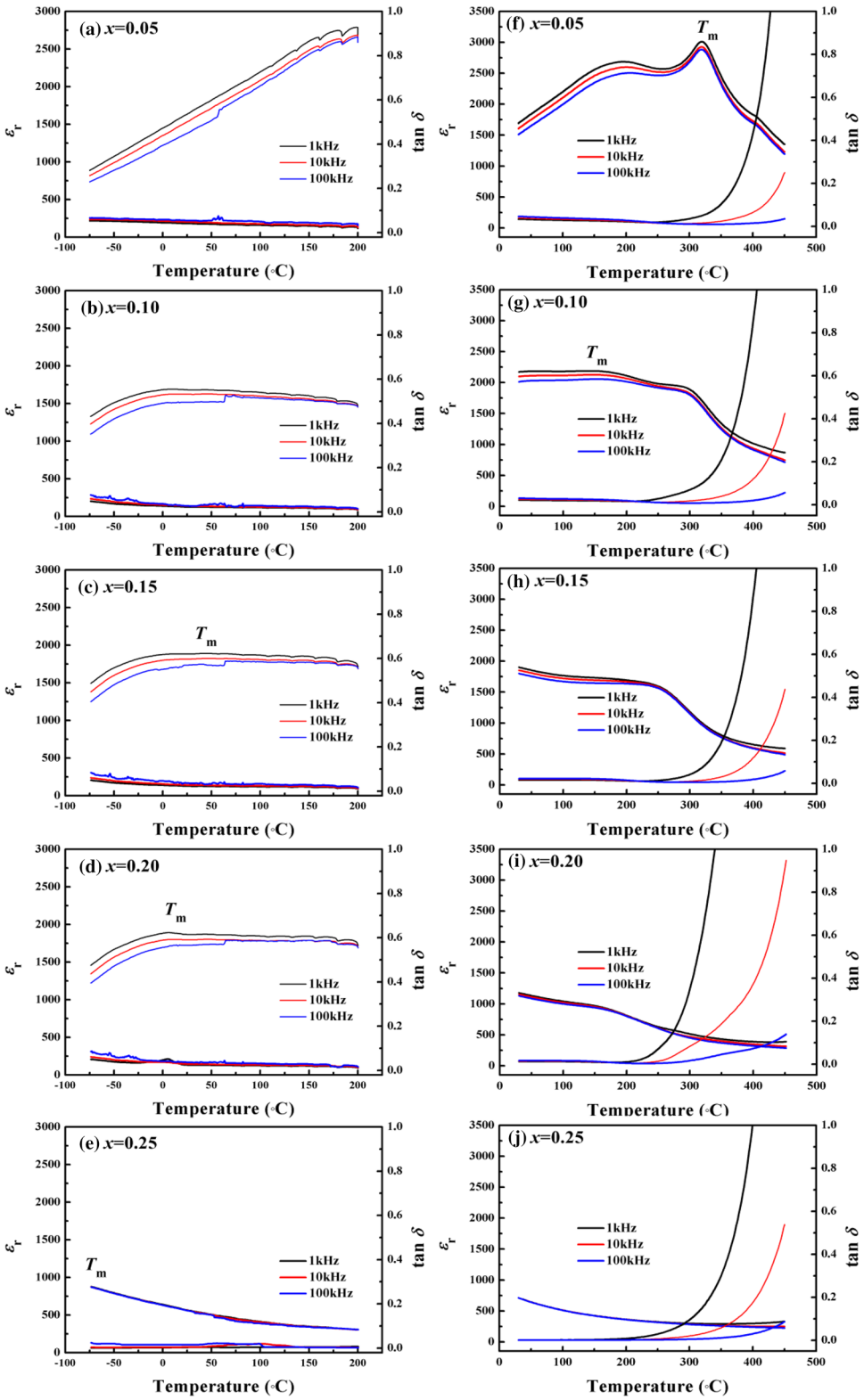

Fig. 5 Temperature dependence of the dielectric constant (ε_r) and dielectric loss (tan δ) for KNN−xSIN ceramics

ceramics was determined to be on the order of − 96 ppm/°C, 277 ppm/°C and 133 ppm/°C, respectively.

Based on the above comprehensive analysis, it can be concluded that KNN−xSIN ceramics with high density, uniformly refined grain, the high symmetric pseudo-cubic structure as well as relaxor characteristics have excellent optical performance. Nevertheless, the relaxor characteristics do not contribute to the improvement of ferroelectric

properties. Figure 6a shows the *P–E* hysteresis loop of KNN−*x*SIN transparent ceramics measured at 1 Hz and ambient temperature. Obviously, the *P–E* loops gradually become slimmer as the amount of SIN increases. As demonstrated in Fig. 6b, an apparently reduced ferroelectrics parameters, i.e. maximum polarization (P_{max} = 3.97 μC/cm^2), remnant polarization (P_r = 0.51 μC/cm^2), and coercive field (E_c = 8.86 kV/cm), were originated from KNN−0.25SIN ceramic (for KNN−0.05SIN, P_{max} = 24.53 μC/cm^2, P_r = 9.32 μC/cm^2, E_c = 13.1 kV/cm), implying that the degradation of ferroelectric properties is serious, which is due to the gradually strengthened relaxor characteristic that leads to an increasing symmetry of crystals with pseudo-cubic structure.

For the relaxor ferroelectrics, the energy storage density can be determined by the *P–E* loops according to the integral equation [35]. The dependence of the energy storage density and direct current (DC) breakdown electric field of KNN−*x*SIN ceramic on the SIN doping content is shown in Fig. 6c. Visibly, the energy storage density goes up initially and decreases later. The energy storage density reaches a maximum of 0.36 J/cm^3 for KNN−0.10SIN ceramic at 70 kV/cm. The relatively low energy storage density may be attributed to the gradually increasing relaxor characteristic that causes a smaller difference between P_{max} and P_r with the addition of SIN. DC breakdown strength of the ceramics rises linearly as a function of SIN content. The KNN−0.25SIN ceramic reaches the maximum value as high as 290 kV/cm eventually. High DC breakdown strength can be induced by smaller grain size and dense microstructure, which is conducive to the excellent energy storage characteristics of KNN-based transparent ceramics.

Figure 7 shows the impedance spectroscopy of KNN−0.25SIN ceramic at temperatures ranging from 100 to 500 °C. As the temperature rises, the Cole–Cole curves have a straight line that gradually turns into a semicircular shape. The radius of the semicircle decreases, and its center also deviates from the real axis, which means that KKN−0.25SIN ceramic exhibits non-Debye relaxation [36, 37]. The radius of the semicircle usually represents the resistance of the ceramics samples. When the temperature rises, the resistance of ceramic decreases, indicating a negative temperature coefficient resistance (NTCR) behavior exists in the high-temperature region. In particular, when the temperature increases to 450 °C, only single semicircular arc can be observed, which is the result of the bulk response [17, 38]. The magnitude of the resistance can be obtained according to the intercept between the semi-circle and the real axis, the resistance value at 450 °C is about 42,000 Ω. As the temperature further rises to 500 °C, the spectrum comprises two semicircular arcs corresponding to grain and grain boundary contributions, which can be equivalent to a cascading two parallel *RC* circuits [38]. Thus, it is possible that the grain and grain boundary effect arising concurrently might be associated with the variation in crystal structure regulated primarily by the thermal state of the sample.

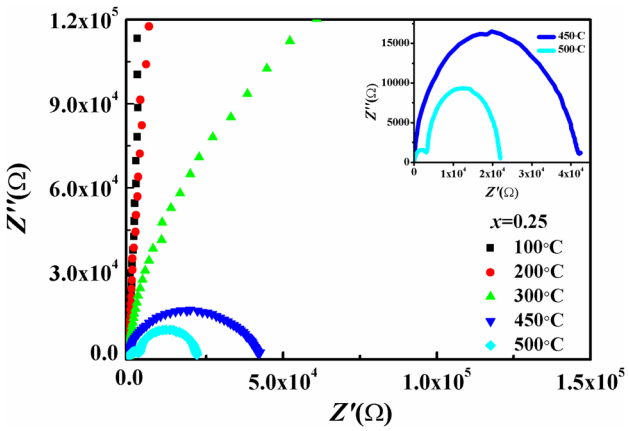

Fig. 7 Impedance spectra of the KNN−0.25SIN ceramic

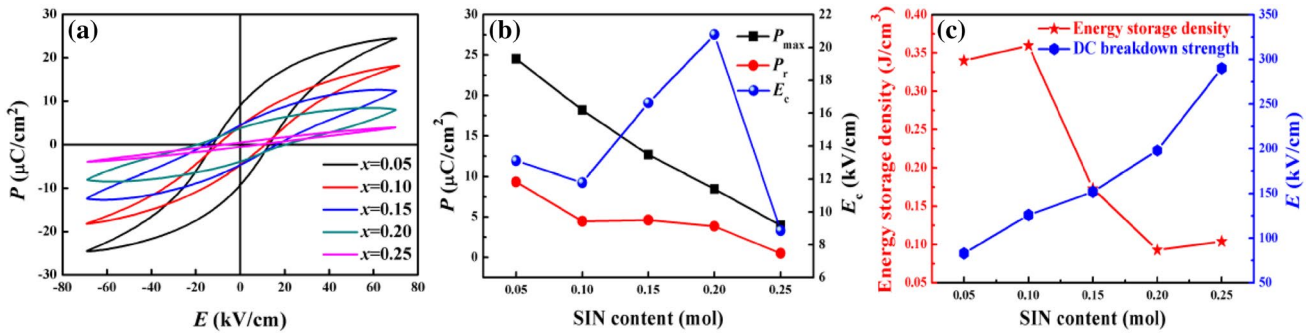

Fig. 6 **a** *P–E* loops, **b** the variation of P_{max}, P_r, and E_c, **c** SIN content dependence of energy storage density and DC breakdown voltage for KNN−*x*SIN ceramics

4 Conclusions

In this work, KNN−*x*SIN transparent ceramics with high optical transmittance and better electrical properties have been fabricated by conventional solid-phase route. The effects of SIN doping concentration on the multifunctional properties of the KNN−*x*SIN were examined. The results indicated that the transmittance of the KNN−*x*SIN ceramics was associated with the symmetric pseudo-cubic structure, fined-grains as well as strengthened relaxor behavior. KNN−0.25SIN ceramic obtained a high visible light transmittance of more than 40%. KNN−*x*SIN ceramics were of typical relaxor ferroelectrics with enhanced temperature stability of dielectric properties. *P–E* loops displayed representative relaxor features accompanied by the energy storage density of 0.36 J/cm^3. High DC breakdown strength of 290 kV/cm implied that a further improvement could be made on the energy storage performance. In addition, KNN−0.25SIN ceramic exhibited non-Debye type relaxation mechanism and NTCR phenomenon with increasing the temperature. The aforementioned effects of microstructure, dielectric, ferroelectric and transparency properties on the KNN−*x*SIN ceramics could provide guidelines to develop the KNN-based transparent electronic ceramics.

Acknowledgements This work is supported by the National Nature Science Foundation of China (11664006, 61741105), Guangxi Nature Science Foundation (2016GXNSFAA380069) and Guangxi Key Laboratory of Information Materials (161001-Z, 171009-Z), Graduate Innovation Research Project of Guilin University of Electronic Technology (2018YJCX81).

References

1. B. Qu, H. Du, Z. Yang, J. Mater. Chem. C. **4**, 1795–1803 (2016)
2. Q. Chai, X. Zhao, X. Chao, Z. Yang, RSC Adv. **7**, 28428–28437 (2017)
3. S.F. Wang, J. Zhang, D.W. Luo, F. Gu, D.Y. Tang, Z.L. Dong, G.E.B. Tan, W.X. Que, T.S. Zhang, S. Li, Prog. Solid State Chem. **41**, 20–54 (2013)
4. G.H. Haertling, C.E. Land, Ferroelectrics **3**, 269–280 (2005)
5. X. Li, Y. Yu, Z. Zheng, Ceram. Int. **42**, 490–494 (2016)
6. K.W. Kwok, F. Li, D. Lin, Funct. Mater. Lett. **4**, 237–240 (2011)
7. M. Kosec, V. Bobnar, M. Hrovat, J. Bernard, B.M.J. Holc, J. Mater. Res. **19**, 1849–1854 (2004)
8. K. Li, F.L. Li, W. Yu, K.W. Kwok, H.L.W. Chan, Mater. Chem. Phys. **131**, 320–324 (2011)
9. F. Li, K.W. Kwok, J. Eur. Ceram. Soc. **33**, 123–130 (2013)
10. J.J. Zhou, J.F. Li, X.W. Zhang, J. Mater. Sci. **47**, 1767–1773 (2012)
11. H. Cheng, W. Zhou, H. Du, F. Luo, D. Zhu, B. Xu, J. Mater. Sci. **49**, 1824–1831 (2014)
12. M. Ichiki, L. Zhang, M. Tanaka, R. Maeda, J. Eur. Ceram. Soc. **24**, 1693–1697 (2004)
13. Y. Chang, S. Poterala, Z. Yang, G.L. Messing, J. Am. Ceram. Soc. **94**, 2494–2498 (2011)
14. F.Z. Yao, K. Wang, J.F. Li, J. Appl. Phys. **113**, 174105 (2013)
15. Y. Chen, D. Xue, Y. Ma, Z. Chen, X. Jiang, G. Liu, X. Liu, Mater. Res. Bull. **84**, 240–244 (2016)
16. D. Yang, C. Ma, Z. Yang, L. Wei, X. Chao, Z. Yang, J. Yang, Ceram. Int. **42**, 4648–4657 (2016)
17. Z. Liu, H. Fan, Y. Zhao, G. Dong, J. Am. Ceram. Soc. **99**, 146–151 (2016)
18. H. Qiao, C. He, Z. Wang, X. Li, Y. Liu, X. Yang, H. Tailor, X. Long, Mater. Des. **117**, 232–238 (2017)
19. Y. Yoneda, K. Suzuya, J. Mizuki, S. Kohara, J. Appl. Phys. **100**, 093521 (2006)
20. Z. Yang, X. Zhang, D. Yang, B. Yang, X. Chao, L. Wei, Z. Yang, J. Am. Ceram. Soc. **99**, 2055–2062 (2016)
21. X. Zhang, D. Yang, Z. Yang, X. Zhao, Q. Chai, X. Chao, L. Wei, Z. Yang, Ceram. Int. **42**, 17963–17971 (2016)
22. Z. Wang, H. Gu, Y. Hu, K. Yang, M. Hu, D. Zhou, J. Guan, CrystEngComm **12**, 3157–3162 (2010)
23. J. Tauc, *The Optical Properties of Solids* (North-Holland Pub, Amsterdam, 1972)
24. E.A. Davi, N.F. Mott, Philos. Mag. **22**, 0903–0922 (1970)
25. C. Lin, X. Wu, M. Lin, Y. Huang, J. Li, J. Alloys Compd. **706**, 156–163 (2017)
26. Z. Liu, H. Fan, S. Lei, J. Wang, H. Tian, Appl. Phys. A **122**, 900 (2016)
27. S. Sang, Z. Yuan, L. Zheng, E. Sun, R. Zhang, J. Wang, R. Wang, B. Yang, M. Liu, Opt. Mater. **45**, 104–108 (2015)
28. D. Yang, Z. Yang, X. Zhang, L. Wei, X. Chao, Z. Yang, J. Alloys Compd. **716**, 21–29 (2017)
29. K. Shalini, G. NambiVenkatesan, Mater. Res. Expr. **5**, 096104 (2018)
30. S. Lee, W.H. Woodford, C.A. Randall, Appl. Phys. Lett. **92**, 1 (2008)
31. S. Anem, K.S. Rao, K.H. Rao, Ceram. Int. **42**, 15319–15326 (2016)
32. R.R. Neurgaonkar, J.R. Oliver, W.K. Cory, L.E. Cross, Mater. Res. Bull. **18**, 735–741 (1983)
33. R.R. Neurgaonkar, J.G. Nelson, J.R. Oliver, L.E. Cross, Mater. Res. Bull. **25**, 959–970 (1990)
34. N. Raengthon, T. Sebastian, D. Cumming, I.M. Reaney, D.P. Cann, J. Am. Ceram. Soc. **95**, 3554–3561 (2012)
35. Y. Zhao, J. Xu, L. Yang, C. Zhou, X. Lu, C. Yuan, Q. Li, G. Chen, H. Wang, J. Alloys Compd. **666**, 209–216 (2016)
36. N. Zidi, A. Chaouchi, S. D'Astorg, M. Rguiti, C. Courtois, J. Alloys Compd. **590**, 557–564 (2014)
37. M. Chandrasekhar, D.K. Khatua, R. Pattanayak, P. Kumar, J. Phys. Chem. Solids **111**, 160–166 (2017)
38. R. Rai, I. Coondoo, S. Sharma, A.L. Kholkin, R. Rani, I. Bdikin, Curr. Appl. Phys. **13**, 430–440 (2013)